Photoacoustics 31 (2023) 100479

Contents lists available at ScienceDirect

Photoacoustics

journal homepage: www.elsevier.com/locate/pacs

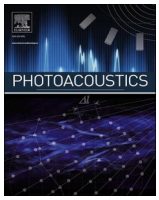

Quartz-enhanced photoacoustic spectroscopy (QEPAS) and Beat Frequency-QEPAS techniques for air pollutants detection: A comparison in terms of sensitivity and acquisition time

Biao Li [a,b,c,1], Giansergio Menduni [c,1], Marilena Giglio [c], Pietro Patimisco [c], Angelo Sampaolo [c], Andrea Zifarelli [c], Hongpeng Wu [a,b,c], Tingting Wei [a,b], Vincenzo Spagnolo [a,c,*], Lei Dong [a,b,c,*]

[a] State Key Laboratory of Quantum Optics and Quantum Optics Devices, Institute of Laser Spectroscopy, Shanxi University, Taiyuan 030006, China
[b] Collaborative Innovation Center of Extreme Optics, Shanxi University, Taiyuan 030006, China
[c] PolySense Lab - Dipartimento Interateneo di Fisica, University and Politecnico of Bari, Via Amendola 173, Bari, Italy

ARTICLE INFO

Keywords:
QEPAS
BF-QEPAS
Air pollutants detection
Multigas measurement
NO detection

ABSTRACT

In this work, a comparison between Quartz Enhanced Photoacoustic Spectroscopy (QEPAS) and Beat Frequency-QEPAS (BF-QEPAS) techniques for environmental monitoring of pollutants is reported. A spectrophone composed of a T-shaped Quartz Tuning Fork (QTF) coupled with resonator tubes was employed as a detection module. An interband cascade laser has been used as an exciting source, allowing the targeting of two NO absorption features, located at 1900.07 cm^{-1} and 1900.52 cm^{-1}, and a water vapor absorption feature, located at 1901.76 cm^{-1}. Minimum detection limits of 90 ppb and 180 ppb were achieved with QEPAS and BF-QEPAS techniques, respectively, for NO detection. The capability to detect multiple components in the same gas mixture using BF-QEPAS was also demonstrated.

1. Introduction

Environmental monitoring of pollutants in the gas phase is critical to safeguard public health, and thus several highly sensitive sensing solutions have been proposed and realized [1–3]. The potentiality to acquire data in wide and harsh environments and to guarantee the safety of the operator promotes Unmanned Aerial Vehicle (UAV)-assisted monitoring as one of the most suitable solutions to trace pollution sources in urban and industrial areas [4]. One of the main requirements concerns data acquisition, which should be reliable and fast at the same time since UAVs are battery-powered and transport heavy payloads. For this reason, UAV-assisted systems require low power consumption, fast response, and compact sensors, capable to validate and transfer data to a ground control station during the operation time. Despite electrochemical and metal-oxide gas sensors have been widely used [5,6], there is a rising interest in the implementation of optical sensors for UAV-assisted monitoring, because of their higher sensitivity and selectivity, also allowing accurate detection of multiple gases in the same mixture [7–9]. Among the different optical techniques [10–22], quartz-enhanced photoacoustic spectroscopy (QEPAS) demonstrated to be suitable and reliable to monitor multiple gas traces in the environment [9,23]. In QEPAS, quartz tuning forks (QTFs) are employed as the detector for sound waves produced by gas molecules when modulated light is absorbed. The direct piezoelectric effect in quartz allows the conversion of the pressure waves into an electric signal. The spectrophone typically employed in QEPAS experiments is composed of a QTF acoustically coupled with a pair of millimetric resonator tubes that amplify acoustic wave intensity between the QTF prongs [24]. Starting from 2002 when the QEPAS technique was first reported [25], several QTF geometries were proposed to improve sensors performances, by optimizing prong spacing, fundamental resonance frequency (f_0), and quality factor (Q) of the QTF [24]. Both f_0 and Q determine the acoustic resonator accumulation time defined as $\tau = Q/(\pi f_0)$ [26]. The spectrophone implementing a T-shaped QTF, with a prong spacing of 0.8 mm, a fundamental resonance frequency of 12.4 kHz, a quality factor Q $>$ 12,000 at atmospheric pressure, and, in turn, an accumulation time of $\sim$ 0.3 s, has been employed in several sensors for in situ pollutants monitoring applications [27–30]. Typically, the photoacoustic signal of

* Corresponding authors at: State Key Laboratory of Quantum Optics and Quantum Optics Devices, Institute of Laser Spectroscopy, Shanxi University, Taiyuan 030006, China.
E-mail addresses: vincenzoluigi.spagnolo@poliba.it (V. Spagnolo), donglei@sxu.edu.cn (L. Dong).
[1] These authors have contributed equally to this work.

https://doi.org/10.1016/j.pacs.2023.100479
Received 10 February 2023; Received in revised form 10 March 2023; Accepted 22 March 2023
Available online 23 March 2023

the gas under investigation is acquired during a slow spectral scan of the laser tuning range across the gas absorption feature, and both the laser modulation and the signal demodulation are carried out at the QTF resonance frequencies or at one of its harmonics. This process could require several minutes and could prevent the real-time monitoring of the QTF resonance parameters, necessary to validate measurements. In 2017, Wu et al. [26] proposed a novel approach, named beat-frequency quartz-enhanced photoacoustic spectroscopy (BF-QEPAS), as an alternative to the QEPAS technique to simultaneously speed up and validate data acquisitions. In BF-QEPAS, the laser modulation frequency (f) is detuned of Δf with respect to the QTF fundamental resonance frequency, and a fast ramp is applied to scan the laser tuning range so that the QTF results excited by an acoustic pulse. As a response, the QTF will relax the accumulated energy with damped oscillations at its natural frequency f_0, with decreasing amplitudes following phenomenologically the exponential law $e^{-t/\tau}$ [26]. Since the response is demodulated at the laser modulation frequency f, the acquired signal will oscillate at the beat frequency $\Delta f = |f - f_0|$ in the Hertz range or lower. The BF-QEPAS signal has already been demonstrated to linearly depend on the gas concentration; in addition, for each excitation pulse, the QTF resonance frequency and the quality factor can be simultaneously retrieved by the analysis of the damped oscillations of the QTF signal in the time domain [26,31].

In this work, a comparison between QEPAS and BF-QEPAS techniques using a T-shaped QTF for nitric oxide (NO) detection was reported by employing an apparatus designed for implementing both techniques. An interband cascade laser (ICL), with a central wavelength of 5.263 μm, allowing both NO and H_2O absorption features to be targeted, was selected as the laser source. NO in the environment is mainly produced by vehicles and industries as a combustion waste of molecular nitrogen in the air at high temperatures [32–34]. The development of sensors for NO concentration monitoring is fundamental to control its presence in the atmosphere, since NO is both an acid rain precursor that contributes to the depletion of ozone in the stratosphere and a precursor of the greenhouse gas nitrous oxide. NO sensors found applications also in the biomedical field since NO is related to the outbreak of respiratory diseases [35–38].

2. Experimental setup

A schematic of the experimental apparatus employed for comparing the QEPAS and BF-QEPAS techniques is shown in Fig. 1.

The acoustic detection module (Thorlabs, mod. ADM01) consisted of a spectrophone enclosed in a compact vacuum-tight gas cell equipped with two windows and inlet/outlet gas connectors. The spectrophone was composed of a T-shaped QTF, resonant at a fundamental frequency of 12.4 kHz, on-beam coupled with acoustic resonator (AR) tubes [39]. A trans-impedance amplifier with a 10 MΩ feedback resistor was employed to transduce the QTF piezoelectric current into a voltage signal. The laser source was an ICL (Nanoplus, mod. 3468/04-28), emitting at a central wavelength of 5.263 μm and with a maximum optical power of 4.68 mW. At a fixed temperature of 14 °C, two NO absorption features, located at 1900.07 cm^{-1} and 1900.52 cm^{-1} with linestrengths of $2.32 \cdot 10^{-20}$ cm/molecule and $1.24 \cdot 10^{-20}$ cm/molecule, respectively, and a water vapor absorption feature, located at 1901.76 cm^{-1} with linestrength of $3.13 \cdot 10^{-22}$ cm/molecule can be targeted within the current dynamic range of the ICL [40]. The laser beam was focused by a convex lens with a focal length of 50 mm between the QTF prongs and through the AR tubes. A power meter was used to control the laser alignment. Laser-injected current and temperature were controlled by a Thorlabs LDC202C current driver and a Thorlabs TED200C temperature controller, respectively. A function generator (Keysight EDU33212A) was employed to generate the modulation signals for the QEPAS and BF-QEPAS configurations. The TTL signal from the function generator was sent to the lock-in amplifier (Synktek, SIGNAL RECOVERY 7625) as a reference signal. The lock-in signal was acquired by a data acquisition card (National Instruments, PCIe-6363) and then transmitted to a personal computer. For all measurements, the signal integration time was set as three times the lock-in time constant. Two gas cylinders, one with a certified concentration of 500 ppm of NO in N_2 and one with standard air (20 % O_2, 1 % H_2O and 79 % N_2), and a gas blender (MCQ instruments, GB100 Series) were used for the generation of different gas mixtures and the calibration of the sensor. A pressure controller (Alicat, EPC-15PSIA-P01), a flow meter (Axetris, MFM 2220-BA-U0), a needle valve, and a vacuum pump were employed to stabilize the pressure and flow rate conditions during the experiment. The flow rate during the experiments was fixed at 50 sccm,

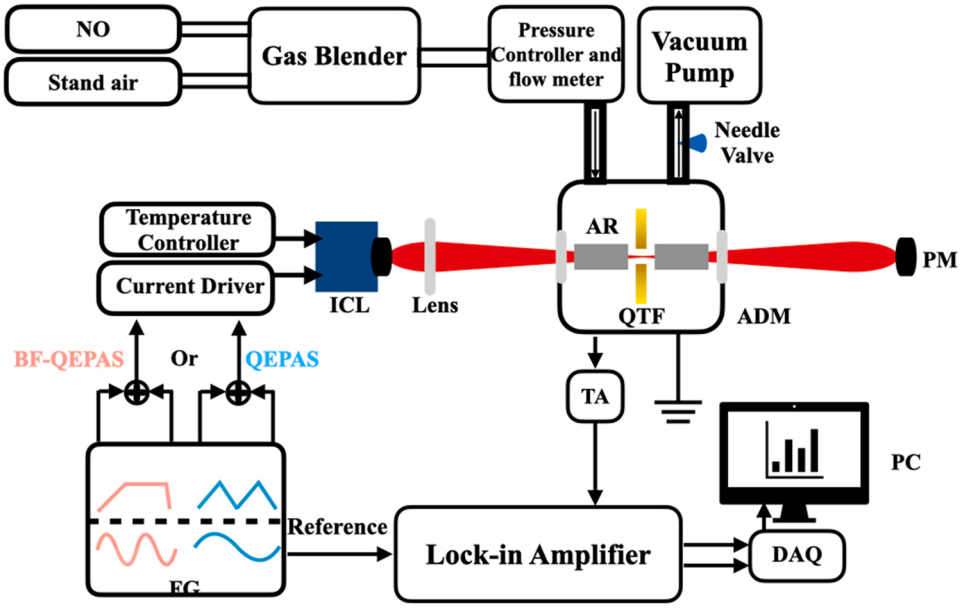

Fig. 1. Schematic of the experimental setup. ICL: interband cascade laser; AR: acoustic resonator; QTF: quartz tuning fork; TA: trans-impedance amplifier; FG: function generator; DAQ: data acquisition card; PC: personal computer, PM: power meter. Red: waveform employed in BF-QEPAS. Blue: waveform employed in standard QEPAS.

while the pressure was varied to optimize the performances for both sensing techniques.

2.1. QEPAS technique

A sinusoidal dither for the wavelength modulation was applied to the laser current driver together with a slow triangle ramp to scan across the current dynamic range of the ICL. The 2*f*-wavelength modulation (2*f*-WM) technique was employed: a sinewave at half of the QTF resonance frequency ($f_0/2$) was provided to the current driver, and the f_0-component of the QTF signal was extracted with the lock-in amplifier. In this way, the 2*f*-signal is not influenced by any background absorption and its maximum value occurs at the peak of the gas absorption feature. Thus, the gas concentration can be directly measured by analyzing the 2*f*-WM QEPAS peak signal [41].

2.2. BF-QEPAS technique

Together with the sinusoidal modulation, a staircase ramp signal was employed for the scanning of the laser current. This signal is composed of a steep rising edge, determining the scan rate of the selected absorption feature in the form of a fast acoustic pulse, followed by a stationary level during which the damped oscillations of the QTF signal can be acquired. In BF-QEPAS, the 1*f*-wavelength modulation (1*f*-WM) technique was employed [26]: a sinewave at a frequency *f* was provided to the current driver, and the QTF signal component at the same frequency was demodulated by the lock-in amplifier. Since the BF-QEPAS sensing performance strongly depends on the modulation frequency, the sinewave frequency *f* was varied to optimize the minimum detection limit (MDL) of the BF-QEPAS sensor.

3. Results and discussion

The BF-QEPAS signal dependence on both the scan rate of the staircase ramp and the lock-in amplifier time constant needs to be investigated to optimize the sensing performance [26]. At the same time, the modulation frequency and amplitude of the sinewave must be optimized for both techniques. The dependence from the above-mentioned parameters was analyzed at three different pressures in the range of 50–700 Torr. In this section, the analysis was carried out by monitoring the signal related to the strongest NO absorption feature, located at 1900.07 cm^{-1}, in a mixture containing 250 ppm of NO in standard air.

3.1. BF-QEPAS scan rate and lock-in time constant optimization

The temporal response of a resonator that is excited by an impulse depends on the accumulation time τ and the time constant of the lock-in amplifier. The BF-QEPAS signal as a function of the scan rate when the lock-in time constant is fixed to 5 ms is shown in Fig. 2 for three different pressure values, namely 100 Torr, 400 Torr, and 700 Torr.

For each investigated pressure value, the BF-QEPAS signal preserves the same trend as a function of the wavelength scan rate, with a well-defined peak value maximizing the signal. Values recorded at 100 Torr are significantly lower with respect to those acquired at higher pressures: this is due to the pressure-dependence of the QEPAS signal resulting in a trade-off between the increase of the QTF quality factor and the reduction of the NO relaxation rate when reducing the pressure [42]. Due to the dependence of the quality factor on the pressure [42], the QTF accumulation time decreases as the pressure increases. For this reason, the optimal wavelength scan rate shifts from 0.0770 $cm^{-1}Hz$ at 100 Torr to higher rates, i.e., 0.592 $cm^{-1}Hz$ at 700 Torr. As a result of Fig. 2, the optimal wavelength scan rate and the optimal working pressure for this BF-QEPAS system resulted in 0.335 $cm^{-1}Hz$ and 400 Torr, respectively.

Fixing the wavelength scan rate at 0.335 $cm^{-1}Hz$, the BF-QEPAS signal was acquired at different lock-in time constants for 100 Torr, 400 Torr, and 700 Torr gas pressures, and the results are shown in Fig. 3.

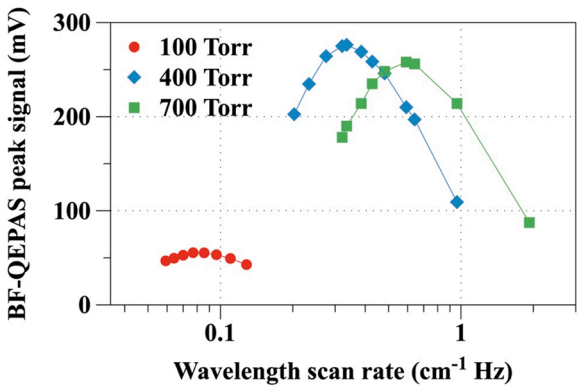

Fig. 2. BF-QEPAS peak signal as a function of the wavelength scan rate acquired at 100 Torr (red dots), 400 Torr (blue diamonds) and 700 Torr (green squares), when a gas mixture with 250 ppm of NO in standard air flows through the acoustic detection module ADM01.

For each gas pressure value, the results show that the BF-QEPAS signal is almost independent by the lock-in time constant up to 10^4 μs; at higher values, it slightly decreases. The optimal time constant maximizing the BF-QEPAS thereby resulted in 5 ms at 400 Torr: this value is significantly lower than 100 ms, which is the time constant typically employed in QEPAS experiments, opening the way to faster measurements.

Finally, the optimized QEPAS and BF-QEPAS signals were acquired in the 50–700 Torr range, with a lock-in time constant set to 100 ms and 5 ms, respectively. The results are shown in Fig. 4.

The QEPAS and BF-QEPAS signal trends are similar: the maximum value was measured at 400 Torr with an optimal sinewave modulation amplitude of 5 mA for both techniques.

3.2. Optimization of modulation frequency

Fig. 5 reports the BF-QEPAS signal as a function of the modulation frequency together with the QTF resonance curve of the fundamental in-plane flexural mode, at 400 Torr.

For the QTF resonance curve, a peak frequency (f_0) of 12439.6 Hz, a quality factor of 13720, and, in turn, an accumulation time of 0.35 s were extracted for the fundamental in-plane flexural mode by the electrical excitation. With respect to the QTF resonance curve, the BF-QEPAS trend exhibits two symmetric sidelobes detuned of $\Delta f = \pm 1.7$ Hz with respect to f_0. The lower frequency ($f = f_0$

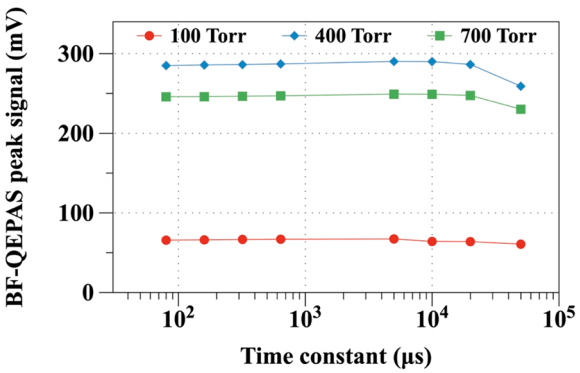

Fig. 3. BF-QEPAS peak signal as a function of the lock-in time constant at 100 Torr (red dots), 400 Torr (blue diamonds) and 700 Torr (green squares), acquired when a gas mixture with 250 ppm of NO in standard air flows through the acoustic detection module ADM01.

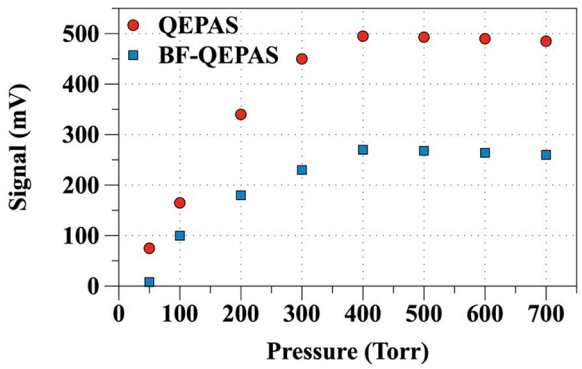

Fig. 4. Optimized QEPAS (red dots) and BF-QEPAS (blue squares) peak signals in the 50–700 Torr pressure range under investigation when a gas mixture with 250 ppm of NO in standard air flows through the acoustic detection module ADM01.

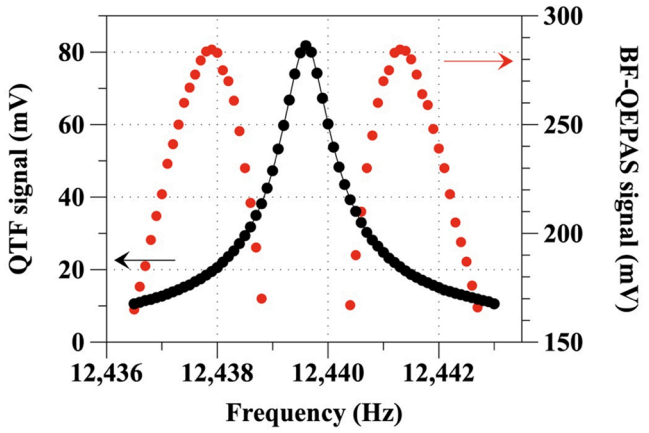

Fig. 5. Red dots: BF-QEPAS peak signal for a gas mixture of 250 ppm of NO in standard air as a function of the laser modulation frequency at 400 Torr. Black dots: Resonance curve at 400 Torr measured electrically exciting the QTF.

$-\Delta f = 12437.9$ Hz) was selected in the calibration phase for the sinusoidal modulation.

3.3. Calibration of the sensing systems and multiple gas detection

As a result of the optimization phase, both techniques were compared at 400 Torr by using different gas mixtures with a 50–300 ppm NO concentration range diluted in standard air for calibration. The signal of the strongest NO absorption line located at 1900.07 cm^{-1} was considered in this phase. Fig. 6(a) shows the QEPAS scans at different NO concentrations.

For each spectral scan, peak values were extracted and plotted as a function of the NO concentration in Fig. 6(b). A detection sensitivity of 2.02 mV/ppm was retrieved from the slope of the linear fit of data points. The noise level was measured by flushing standard air through the acoustic detection module and acquiring the 1σ standard deviation of the signal, while the laser emission was fixed at the NO absorption line (slow triangle ramp off). The measured QEPAS noise was 0.18 mV, leading to an MDL of 90 ppb and to a normalized noise equivalent absorption (NNEA) value of $5.9{\cdot}10^{-9}$ cm^{-1} W $Hz^{-1/2}$.

The BF-QEPAS signals measured for different NO concentrations are reported in Fig. 7(a).

The calibration curve in Fig. 7(b) was obtained by extracting the value of the first positive peak (labeled as P1 in Fig. 7(a)) for each NO concentration. These values were plotted as a function of the NO concentration in Fig. 7(b). The slope of the linear fit of data points returns a BF-QEPAS sensitivity of 1.16 mV/ppm. Similarly to QEPAS, for BF-QEPAS the noise signal was measured by flushing standard air and acquiring the 1σ standard deviation of the signal, keeping the laser emission at the NO absorption line. The measured noise level resulted in 0.21 mV, leading to an MDL of 180 ppb and to a NNEA value of $2.5{\cdot}10^{-9}$ cm^{-1} W $Hz^{-1/2}$. Considering the BF model presented in [31], the number of peaks (n_{peaks}) in Fig. 7(a) can be estimated as

$$n_{peaks} = \Delta f \cdot t_{noise}$$

where Δf is the beat frequency optimizing the BF-QEPAS signal (shown in Fig. 5) and t_{noise} is the time needed to reach the noise level, calculated as

$$t_{noise} = \tau \cdot \ln(V_{peak}/v_{noise})$$

where τ is the accumulation time of the QTF, V_{peak} is the peak value of P1 and v_{noise} is the measured noise level.

For each NO concentration, the five positive peaks (P1–P5 in Fig. 7(a)) can be employed to determine both the resonance frequency and the quality factor of the QTF. The time intervals between the five peaks were employed to calculate the inverse of beat frequency Δf. Then, the QTF resonance frequency can be retrieved as $f_0 = f + \Delta f = 12439.6$ Hz. An exponential fit $e^{-t/\tau}$ of the five peaks was used to estimate the QTF accumulation time τ and retrieve its quality factor. As shown in Table 1, the calculated resonance frequency is very accurate, and the mean value and the standard deviation of the estimated quality factor are 13078 and 152, respectively, corresponding to a relative error of 1.1 %. Such a relative error is largely within the error bar of parameters extracted from the fitting procedure and used for the estimation of the quality factor. Both f_0 and Q retrieved from the BF-QEPAS signal can be employed to validate the measurements.

A full scan of the laser tuning range was performed in order to detect

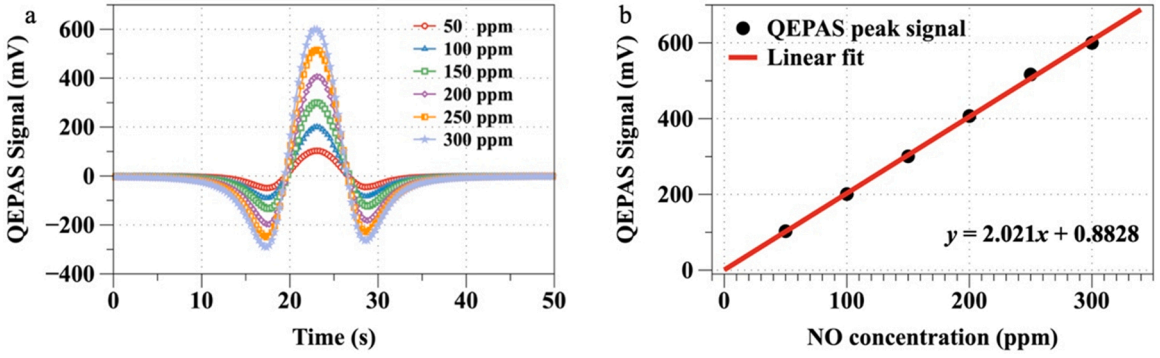

Fig. 6. (a) QEPAS spectral scans measured for different NO concentrations in standard air. (b) QEPAS peak values were plotted as a function of the NO concentration (black dots). The red solid line is the best linear fit of the experimental data.

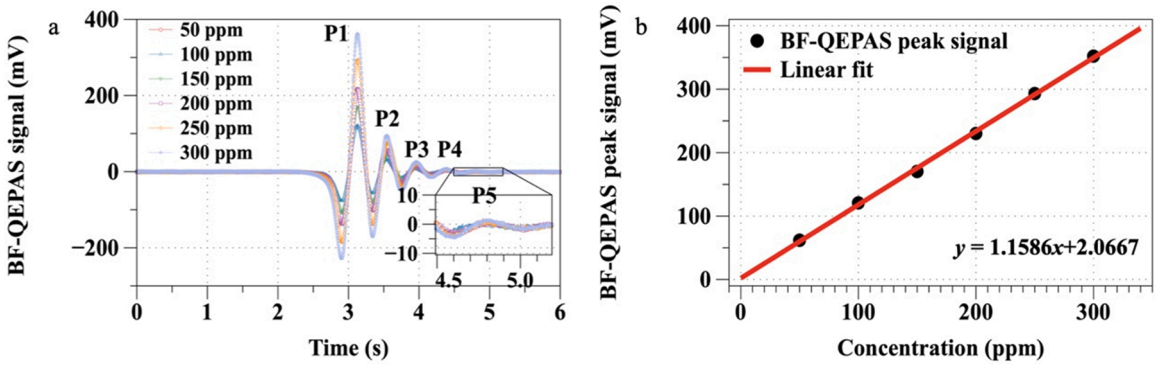

Fig. 7. (a) BF-QEPAS spectral scans measured for different NO concentrations in standard air. (b) BF-QEPAS P1 values were plotted as a function of the NO concentration (black dots). The red solid line is the best linear fit of the experimental data.

Table 1
QTF fitting parameters at different concentrations of NO.

Concentration	50 ppm	100 ppm	150 ppm	200 ppm	250 ppm	300 ppm
f_0(Hz)	12439.6	12439.6	12439.6	12439.6	12439.6	12439.6
Q	13052	12896	13091	13209	12935	13287

both the water vapor and nitric oxide in a mixture composed of 250 ppm of NO in standard air. The acquired QEPAS spectrum is shown in Fig. 8.

As expected, the 250 s-long spectral scan resolves three well-isolated 2*f*-absorption features. The first feature at 22 s with a peak value of ~ 9 mV (see the inset in Fig. 8) is related to the water vapor absorption line located at 1901.76 cm^{-1}. The second and the third features at 160 s and 205 s with peak values of ~ 220 mV and ~ 520 mV correspond to the NO absorption lines located at 1900.52 cm^{-1} at 1900.07 cm^{-1}, respectively. The same scan was investigated with the BF-QEPAS technique, and the acquired spectrum is shown in Fig. 9.

The same time constant employed in the NO calibration was used. The staircase ramp was optimized to fully scan the spectral range and well-resolve the three transient responses: three stationary levels of the ramp were employed while keeping the same scan rate optimized for the detection of NO. The first signal, in the time range from 2 s to 5 s and with a maximum value of ~ 16 mV, corresponds to the H_2O absorption feature at 1901.76 cm^{-1} (see the inset in Fig. 9). The second and the third signals, fall in the respective time ranges from 6 s to 9 s and from 10 s to 13 s and with respective maximum values of ~ 110 mV and ~ 290 mV, corresponding to the two selected NO absorption features at 1900.52 cm^{-1} and 1900.07 cm^{-1}, respectively. The analysis of the measured BF-signals returned a resonance frequency and a quality factor of 12439.6 ± 0.1 Hz and 13140 ± 140 (i.e., 1 %), respectively, in excellent agreement with the same parameters measured from the QTF characterization (Fig. 5). BF-QEPAS allows the reduction of the overall

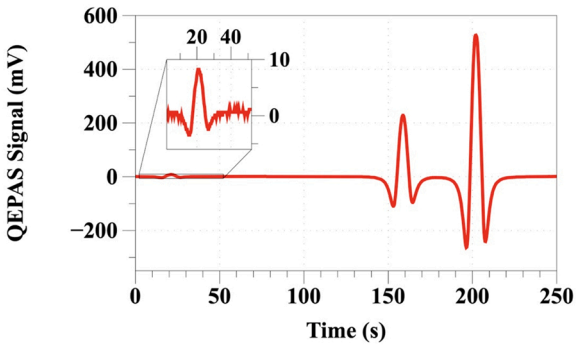

Fig. 8. QEPAS signal for a gas mixture with 250 ppm of NO in standard air in the full laser tuning range.

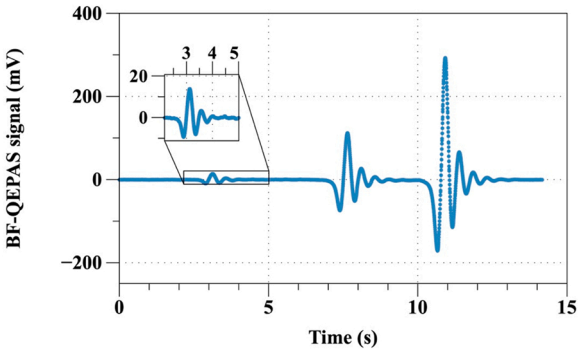

Fig. 9. BF-QEPAS signal for a gas mixture with 250 ppm of NO in standard air in the full laser tuning range.

scanning time of more than one order of magnitude, from 250 s (QEPAS technique) to 14 s.

4. Conclusions

In this work, a comparison between QEPAS and BF-QEPAS techniques for environmental monitoring applications was reported. The spectrophone was composed of a custom T-shaped QTF resonating at 12.4 kHz, coupled with two acoustic resonator tubes. Both NO and H_2O were detected in the same gas mixture, employing an ICL emitting at a central wavelength of 5.263 μm. Considering the selected NO absorption feature at 1900.07 cm^{-1},a MDL of 90 ppb and a NNEA of $5.9{\cdot}10^{-9}$ cm^{-1} W $Hz^{-1/2}$ were achieved using the QEPAS system, corresponding to a lock-in time constant of 100 ms. The BF-QEPAS system reaches an NO MDL of 180 ppb and a NNEA of $2.5{\cdot}10^{-9}$ cm^{-1} W $Hz^{-1/2}$, corresponding to a lock-in time constant of 5 ms.

BF-QEPAS is characterized by a slightly lower performance in terms of detection limit, but, considering the much short measurement time required, shows a better NNEA value and allows a validation of the measurement by monitoring the spectrophone resonance properties, with a respective accuracy on the resonance frequency and quality factor of 0.1 Hz and 1 %. Furthermore, the possibility to detect both NO and H_2O in a gas mixture was demonstrated. With respect to standard QEPAS, the BF-QEPAS technique reduces the overall scanning time by a

factor of ~ 18, requiring less than 15 s to scan three different absorption features and a few seconds for each of them. These results promote BF-QEPAS as a cutting-edge technique for environmental monitoring of pollutants with UAV-assisted technology, requiring fast measurements and data communication with ground control stations or when the rapid variation of the NO concentration is expected. A study on the humidity effect on both QEPAS and BF-QEPAS signals will be carried out to further compare both techniques [9,43]. Finally, the spectrophone structure and its front-end electronics could be further optimized for the BF-QEPAS technique, thus reducing the minimum detection limit difference with the QEPAS technique.

Declaration of Competing Interest

The authors declare that they have no known competing financial interests or personal relationships that could have appeared to influence the work reported in this paper.

Data Availability

Data will be made available on request.

Acknowledgements

The project is sponsored by National Key R&D Program of China (No. 2019YFE0118200); National Natural Science Foundation of China (NSFC) (Nos. 62235010, 62175137, 62122045, 62075119); The Shanxi Science Fund for Distinguished Young Scholars (20210302121003); the Open Fund of the State Key Laboratory of Integrated Optoelectronics, China (No. IOSKL2020KF10). Biao Li acknowledges financial support from the program of China Scholarship Council (No. 202108140145). Dr. Giansergio Menduni acknowledges financial support from the Fondo Sociale Europeo REACT EU—Programma Operativo Nazionale Ricerca e Innovazione 2014–2020 by Ministero dell'Università e della Ricerca, Italy, Code: D95F21002140006. The authors from Dipartimento Interateneo di Fisica di Bari acknowledge financial support from PNRR MUR Project PE0000023-NQSTI, the European Union's Horizon 2020 Research and Innovation Program under grant agreement (No. 101016956 PASSEPARTOUT) and THORLABS GmbH within the Poly-SenSe Joint Research Laboratory.

References

[1] Y. Liu, H. Lin, B.A.Z. Montano, W. Zhu, Y. Zhong, R. Kan, B. Yuan, J. Yu, M. Shao, H. Zheng, Integrated near-infrared QEPAS sensor based on a 28 kHz quartz tuning fork for online monitoring of CO_2 in the greenhouse, Photoacoustics 25 (2022), 100332.

[2] X. Yin, M. Gao, R. Miao, L. Zhang, X. Zhang, L. Liu, X. Shao, F.K. Tittel, Near-infrared laser photoacoustic gas sensor for simultaneous detection of CO and H_2S, Opt. Express 29 (2021) 34258.

[3] S. Li, L. Dong, H. Wu, A. Sampaolo, P. Patimisco, V. Spagnolo, F.K. Tittel, Ppb-level quartz-enhanced photoacoustic detection of carbon monoxide exploiting a surface grooved tuning fork, Anal. Chem. 91 (2019) 5834–5840.

[4] A. Fascista, Toward integrated large-scale environmental monitoring using WSN/UAV/crowdsensing: a review of applications, signal processing, and future perspectives, Sensors 22 (2022) 1824.

[5] M. Kaliszewski, M. Włodarski, J. Młyńczak, B. Jankiewicz, L. Auer, B. Bartosewicz, M. Liszewska, B. Budner, M. Szala, B. Schneider, G. Povoden, K. Kopczyński, The multi-gas sensor for remote UAV and UGV missions—development and tests, Sensors 21 (2021) 7608.

[6] J. Burgués, M.D. Esclapez, S. Doñate, L. Pastor, S. Marco, Aerial mapping of odorous gases in a wastewater treatment plant using a small drone, Remote Sens. 13 (2021) 1757.

[7] T. Gardiner, M.I. Mead, S. Garcelon, R. Robinson, N. Swann, G.M. Hansford, P. T. Woods, R.L. Jones, A lightweight near-infrared spectrometer for the detection of trace atmospheric species, Rev. Sci. Instrum. 81 (2010), 083102.

[8] L.M. Golston, L. Tao, C. Brosy, K. Schäfer, B. Wolf, J. McSpiritt, B. Buchholz, D. R. Caulton, D. Pan, M.A. Zondlo, D. Yoel, H. Kunstmann, M. McGregor, Lightweight mid-infrared methane sensor for unmanned aerial systems, Appl. Phys. B 123 (2017) 170.

[9] A. Sampaolo, P. Patimisco, M. Giglio, A. Zifarelli, H. Wu, L. Dong, V. Spagnolo, Quartz-enhanced photoacoustic spectroscopy for multi-gas detection: a review, Anal. Chim. Acta 1202 (2022), 338894.

[10] L.E. Mchale, B. Martinez, T.W. Miller, A.P. Yalin, Open-path cavity ring-down methane sensor for mobile monitoring of natural gas emissions, Opt. Exp. 27 (2019) 20084.

[11] Q. He, C. Zheng, K. Zheng, F.K. Tittel, Off-axis integrated cavity output spectroscopy for real-time methane measurements with an integrated wavelength-tunable light source, Infrared Phys. Technol. 115 (2021), 103705.

[12] C. Li, L. Dong, C. Zheng, F.K. Tittel, Compact TDLAS based optical sensor for ppb level ethane detection by use of a 3.34 μm room-temperature CW interband cascade laser, Sens. Actuators B Chem. 232 (2016) 188–194.

[13] Z. Li, Z. Wang, C. Wang, W. Ren, Optical fiber tip-based quartz-enhanced photoacoustic sensor for trace gas detection, Appl. Phys. B 122 (2016) 147.

[14] K. Chen, B. Zhang, M. Guo, Y. Chen, H. Deng, B. Yang, S. Liu, F. Ma, F. Zhu, Z. Gong, Q. Yu, Photoacoustic trace gas detection of ethylene in high-concentration methane background based on dual light sources and fiber-optic microphone, Sens. Actuators B Chem. 310 (2020), 127825.

[15] K. Liu, L. Dong, F.K. Tittel, Compact sound-speed sensor for quartz enhanced photoacoustic spectroscopy based applications, Rev. Sci. Instrum. 86 (2015), 044903.

[16] K. Zheng, L. Yu, C. Zheng, Z. Xi, Y. Zhang, G. Yan, H. Zhang, Y. Zhang, Y. Wang, F. K. Tittel, Vehicle-deployed off-axis integrated cavity output spectroscopic CH_4/C_2H_6 sensor system for mobile inspection of natural gas leakage, ACS Sens. 7 (2022) 1685–1697.

[17] X. Xue, J. Xiao, Y. Tian, H. Ye, X. Wang, High-sensitivity all-optical PA spectrometer based on fast swept laser interferometry, Photoacoustics 28 (2022), 100391.

[18] Z. Lang, S. Qiao, Y. He, Y. Ma, Quartz tuning fork-based demodulation of an acoustic signal induced by photo-thermo-elastic energy conversion, Photoacoustics 22 (2021), 100272.

[19] X. Liu, S. Qiao, G. Han, J. Liang, Y. Ma, Highly sensitive HF detection based on absorption enhanced light-induced thermoelastic spectroscopy with a quartz tuning fork of receive and shallow neural network fitting, Photoacoustics 28 (2022), 100422.

[20] C. Zhang, S. Qiao, Y. Ma, Highly sensitive photoacoustic acetylene detection based on differential photoacoustic cell with retro-reflection-cavity, Photoacoustics 30 (2023), 100467.

[21] S. Qiao, A. Sampaolo, P. Patimisco, V. Spagnolo, Y. Ma, Ultra-highly sensitive HCl-LITES sensor based on a low-frequency quartz tuning fork and a fiber-coupled multi-pass cell, Photoacoustics 27 (2022), 100381.

[22] Y. Ma, Y. Hu, S. Qiao, Z. Lang, X. Liu, Y. He, V. Spagnolo, Quartz tuning forks resonance frequency matching for laser spectroscopy sensing, Photoacoustics 25 (2022), 100329.

[23] G. Menduni, A. Zifarelli, A. Sampaolo, P. Patimisco, M. Giglio, N. Amoroso, H. Wu, L. Dong, R. Bellotti, V. Spagnolo, High-concentration methane and ethane QEPAS detection employing partial least squares regression to filter out energy relaxation dependence on gas matrix composition, Photoacoustics 26 (2022), 100349.

[24] L. Dong, A.A. Kosterev, D. Thomazy, F.K. Tittel, QEPAS spectrophones: design, optimization, and performance, Appl. Phys. B 100 (2010) 627–635.

[25] A.A. Kosterev, Y.A. Bakhirkin, R.F. Curl, F.K. Tittel, Quartz-enhanced photoacoustic spectroscopy, Opt. Lett. 27 (2002) 1902–1904.

[26] H. Wu, L. Dong, H. Zheng, Y. Yu, W. Ma, L. Zhang, W. Yin, L. Xiao, S. Jia, F. K. Tittel, Beat frequency quartz-enhanced photoacoustic spectroscopy for fast and calibration-free continuous trace-gas monitoring, Nat. Commun. 8 (2017) 15331.

[27] A. Zifarelli, R. De Palo, P. Patimisco, M. Giglio, A. Sampaolo, S. Blaser, J. Butet, O. Landry, A. Müller, V. Spagnolo, Multi-gas quartz-enhanced photoacoustic sensor for environmental monitoring exploiting a Vernier effect-based quantum cascade laser, Photoacoustics 28 (2022), 100401.

[28] G. Menduni, A. Zifarelli, E. Kniazeva, S. Dello Russo, A.C. Ranieri, E. Ranieri, P. Patimisco, A. Sampaolo, M. Giglio, F. Manassero, E. Dinuccio, G. Provolo, H. Wu, D. Lei, V. Spagnolo, Measurement of methane, nitrous oxide and ammonia in atmosphere with a compact quartz-enhanced photoacoustic sensor, Sens. Actuators B Chem. 375 (2023), 132953.

[29] A. Zifarelli, G. Menduni, M. Giglio, A. Elefante, A. Sukhinets, A. Sampaolo, P. Patimisco, S. Fangyuan, W. Chongwu, Q.J. Wang, V. Spagnolo, Compact and versatile QEPAS-based sensor box for simultaneous detection of methane and infrared absorber gas molecules in ambient air, Front. Environ. Chem. 3 (2022), 926233.

[30] ⟨https://www.thorlabs.com/newgrouppage9.cfm?objectgroup_id=11241⟩.

[31] T. Wei, A. Zifarelli, S. Dello Russo, H. Wu, G. Menduni, P. Patimisco, A. Sampaolo, V. Spagnolo, L. Dong, High and flat spectral responsivity of quartz tuning fork used as infrared photodetector in tunable diode laser spectroscopy, Appl. Phys. Rev. 8 (2021), 041409.

[32] Y. Jin, M.C. Veiga, C. Kennes, Bioprocesses for the removal of nitrogen oxides from polluted air, J. Chem. Technol. Biotechnol. 80 (2005) 483–494.

[33] T. Boningari, P.G. Smirniotis, Impact of nitrogen oxides on the environment and human health: Mn-based materials for the NOx abatement, Curr. Opin. Chem. Eng. 13 (2016) 133–141.

[34] United States Environmental Protection Agency, Office Of Air Quality Planning And Standards, National Air Pollutant Emission Trends, –1998: U.S. Epa and the States–working Together for Cleaner Air!, U.S. Environmental Protection Agency, Office of Air Quality, Planning and Standards, Research Triangle Park, NC, 2000. [Pdf] Retrieved from the Library of Congress, ⟨https://www.loc.gov/item/00327858/⟩.

[35] C.T. Bowman, Control of combustion-generated nitrogen oxide emissions: technology driven by regulation, in: Proceedings of the Twenty-Fourth Symposium (International) on Combustion/The Combustion Institute, 1992, pp. 859–78.

[36] J.L. Peel, R. Haeuber, V. Garcia, A.G. Russell, L. Neas, Impact of nitrogen and climate change interactions on ambient air pollution and human health, Biogeochemistry 114 (2013) 121–134.
[37] M. Janette, Vincent, diffuse lung disorders — a comprehensive clinical-radiological overview, Australas. Radiol., 2002.
[38] T.W. Group, Pollution Prevention and Abatement Handbook 1998: Toward Cleaner Production, World Bank Group, 1999.
[39] P. Patimisco, A. Sampaolo, M. Giglio, S. Dello Russo, V. Mackowiak, H. Rossmadl, A. Cable, F.K. Tittel, V. Spagnolo, Tuning forks with optimized geometries for quartz-enhanced photoacoustic spectroscopy, Opt. Exp. 27 (2019) 1401.
[40] I.E. Gordon, L.S. Rothman, R.J. Hargreaves, R. Hashemi, E.V. Karlovets, F. M. Skinner, E.K. Conway, C. Hill, R.V. Kochanov, Y. Tan, P. Wcisło, A.A. Finenko, K. Nelson, P.F. Bernath, M. Birk, V. Boudon, A. Campargue, K.V. Chance, A. Coustenis, B.J. Drouin, J. –M. Flaud, R.R. Gamache, J.T. Hodges, D. Jacquemart, E.J. Mlawer, A.V. Nikitin, V.I. Perevalov, M. Rotger, J. Tennyson, G.C. Toon, H. Tran, V.G. Tyuterev, E.M. Adkins, A. Baker, A. Barbe, E. Canè, A.G. Császár, A. Dudaryonok, O. Egorov, A.J. Fleisher, H. Fleurbaey, A. Foltynowicz, T. Furtenbacher, J.J. Harrison, J. –M. Hartmann, V. –M. Horneman, X. Huang, T. Karman, J. Karns, S. Kassi, I. Kleiner, V. Kofman, F. Kwabia–Tchana, N. N. Lavrentieva, T.J. Lee, D.A. Long, A.A. Lukashevskaya, O.M. Lyulin, V. Yu Makhnev, W. Matt, S.T. Massie, M. Melosso, S.N. Mikhailenko, D. Mondelain, H. S.P. Müller, O.V. Naumenko, A. Perrin, O.L. Polyansky, E. Raddaoui, P.L. Raston, Z. D. Reed, M. Rey, C. Richard, R. Tóbiás, I. Sadiek, D.W. Schwenke, E. Starikova, K. Sung, F. Tamassia, S.A. Tashkun, J. Vander Auwera, I.A. Vasilenko, A.A. Vigasin, G.L. Villanueva, B. Vispoel, G. Wagner, A. Yachmenev, S.N. Yurchenko, The HITRAN2020 molecular spectroscopic database, J. Quant. Spectrosc. R. A 277 (2022), 107949.
[41] R. Engelbrecht, A compact NIR fiber-optic diode laser spectrometer for CO and CO_2, Spectrochim. Acta A Mol. Biomol. Spectrosc. 60 (2004) 3291–3298.
[42] P. Patimisco, A. Sampaolo, V. Mackowiak, H. Rossmadl, A. Cable, F.K. Tittel, V. Spagnolo, Loss mechanisms determining the quality factors in quartz tuning forks vibrating at the fundamental and first overtone modes, IEEE Trans. Ultrason. Ferroelectr. Freq. Control 65 (2018) 1951–1957.
[43] Y. Cao, R. Wang, J. Peng, K. Liu, W. Chen, G. Wang, X. Gao, Humidity enhanced N_2O photoacoustic sensor with a 4.53 μm quantum cascade laser and Kalman filter, Photoacoustics 24 (2021), 100303.

Biao Li is now pursuing a Ph.D. degree in atomic and molecular physics in the Institute of Laser Spectroscopy of Shanxi University, China. His research interests include gas sensors, photoacoustic spectroscopy, and laser spectroscopy techniques.

Giansergio Menduni received the M.S. degree (cum laude) in Electronic Engineering in 2017 from the Technical University of Bari. Since 2018, he is a Ph.D. student at the Electric and Information Engineering Department of Polytechnic of Bari. Since 2022, he is an Assistant Professor in Applied Physics at the Physics Department of Polytechnic of Bari. His research activity is focused on the development of gas sensors based on Quartz Enhanced Photoacoustic Spectroscopy.

Marilena Giglio received the M.S. degree (cum laude) in Applied Physics in 2014, and the Ph.D. Degree in Physics in 2018 from the University of Bari. Since 2021, she is a Assistant Professor at the Physics Department of the Technical University of Bari. Her research activity is focused on the development of gas sensors based on Quartz-Enhanced Photoacoustic Spectroscopy and on the optical coupling of hollow-core waveguides with interband- and quantum-cascade lasers.

Pietro Patimisco obtained the Master degree in Physics (cum laude) in 2009 and the Ph.D. Degree in Physics in 2013 from the University of Bari. Since 2018, he is Assistant professor at the Technical University of Bari. Dr. Patimisco's scientific activity addressed the study and applications of trace-gas sensors, such as quartz-enhanced photoacoustic spectroscopy and cavity enhanced absorption spectroscopy in the mid infrared and terahertz spectral region, leading to several publications.

Angelo Sampaolo obtained his Master degree in Physics in 2013 and the Ph.D. Degree in Physics in 2017 from University of Bari. He was an associate researcher in the Laser Science Group at Rice University from 2014 to 2016 and associate researcher at Shanxi University since 2018. Since 2019, he is Assistant Professor at Polytechnic of Bari. His research activity has focused on the development of innovative techniques in trace gas sensing, based on Quartz-Enhanced Photoacoustic Spectroscopy and covering the full spectral range from near-IR to THz.

Andrea Zifarelli obtained his M.S. degree (cum laude) in Physics in 2018 from the University of Bari. From the same year, he is a Ph.D. student at the Physics Department of the University of Bari, developing his research work at PolySense Lab, joint-research laboratory between Technical University of Bari and THORLABS GmbH. Currently, his research activities are focused on the development of gas sensors based on Quartz-Enhanced Photoacoustic Spectroscopy for detection of gas mixtures and broadband absorbers, exploiting non-conventional laser sources.

Hongpeng Wu received his Ph.D. degree in atomic and molecular physics from Shanxi University, China, in 2017. From September, 2015 to October, 2016, he studied as a joint Ph.D. student in the Electrical and Computer Engineering Department and Rice Quantum Institute, Rice University, Houston, USA. Currently he is a professor in the Institute of Laser Spectroscopy of Shanxi University. His research interests include gas sensors, photoacoustic spectroscopy, photothermal spectroscope and laser spectroscopy techniques.

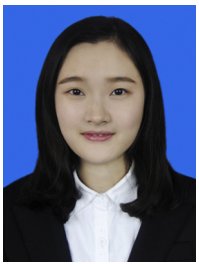

Tingting Wei received her undergraduate degree from Taiyuan University of Science and Technology in July 2017, and entered Shanxi University in September 2017 to pursue a master's degree and a doctorate degree. His research interests include Quartz-Enhanced Photoacoustic Spectroscopy and Quartz-Enhanced Photothermal Spectroscopy. Recently, her research interest has focused on the development of photothermal detector technology based on quartz tuning forks.

Spagnolo Vincenzo received the degree (summa cum laude) and the Ph.D., both in physics, from University of Bari. He works as Full Professor of Applied Physics at the Technical University of Bari. In 2019, he become Vice-Rector of the Technical University of Bari, deputy to Technology Transfer. Since 2017, he is the director of the joint-research lab PolySense, created by THORLABS GmbH and Technical University of Bari, devoted to the development and implementation of novel gas sensing techniques and the realization of highly sensitive QEPAS trace-gas sensors.

Lei Dong received his Ph.D. degree in optics from Shanxi University, China, in 2007. From June, 2008 to December, 2011, he worked as a post-doctoral fellow in the Electrical and Computer Engineering Department and Rice Quantum Institute, Rice University, Houston, USA. Currently he is a professor in the Institute of Laser Spectroscopy of Shanxi University. His research interests include optical sensors, trace gas detection, photoacoustic spectroscopy and laser spectroscopy.